Evaluation of Frequency Regulation Provision by Commercial Building HVAC Systems

Yang Liu[1,2], Nanpeng Yu[1,*], Jie Shi[1], Bing Dong[3], Wei Ren[1], and Xiaohong Guan[2]

Abstract— This paper develops a two-step procedure for commercial buildings to optimize the frequency regulation service provision by leveraging the heating, ventilation, and air conditioning (HVAC) systems. Both day-ahead and real-time operations of the HVAC system are simulated by using a typical commercial building's model, the PJM market prices, and dynamic regulation signals. The simulation results show that it is beneficial for buildings to provide dynamic regulation services where the capacity reserved for regulation up and down are the same. The mean reverting characteristic of the dynamic regulation signal enables commercial buildings to increase regulation capacity with minimal impact on the comfort level of occupants. The proposed frequency regulation provisioning scheme yields a high performance score (>0.9). The simulation results also reveal that there exists a trade-off between frequency regulation performance and climate control performance of the building. Finally, the economic benefits of frequency regulation provisions of commercial buildings are analyzed.

I. INTRODUCTION

The increasing penetration of renewable energy resources introduces greater variability and uncertainty to the supply side of the power system. Therefore, large amounts of ancillary services need to be procured in the electricity market to maintain the reliability of the electric grid. In particular, additional frequency regulation services are needed to handle post real-time dispatch variability and uncertainties stemming from intermittent wind and solar generation resources. Traditionally, frequency regulation services are provided by fossil-fueled generators, which cannot track the fast-changing automatic generation control (AGC) signals very well due to the slower ramp rates [1]. Instead of solely relying on supply-side resources to provide frequency regulation service, HVAC systems of buildings can also be controlled to follow AGC signals. The large thermal inertia and fast ramping rates of supply air fans make building HVAC systems a great candidate for frequency regulation service provision. Furthermore, building electricity loads account for around 70% of total electricity consumption in the U.S. HVAC systems consume around 50% of a building's electricity load [2]. Hence, buildings have an enormous potential to provide a significant portion of the frequency regulation service needs in the electricity market.

[1]Electrical and Computer Engineering, University of California, Riverside
[2]Ministry of Education Key Lab for Intelligent Networks and Network Security (MOE KLINNS), Xi'an Jiaotong University, Xi'an, China
[3]Mechanical Engineering, University of Texas at San Antonio
[*]Corresponding author: Nanpeng Yu (email: nyu@ece.ucr.edu).

Commercial buildings are better suited for providing frequency regulation services than residential buildings for three main reasons: 1) commercial buildings have much larger thermal inertia and higher frequency regulation capacities; 2) many commercial buildings are equipped with energy management system (EMS) which can be configured to receive dispatch signals from the market operators and determine the optimal control trajectory for the building; 3) the majority of commercial building HVAC systems are equipped with variable frequency drives (VFDs) which can adjust the power consumptions of fans and pumps quickly and continuously. Therefore, the supply air fans with VFDs are chosen in this paper to provide frequency regulation services.

Commercial buildings as providers of frequency regulation services have been well studied. Unlike on-off control in residential buildings, the control strategies for HVAC systems in commercial buildings are much more complex. In commercial buildings, various subunits of the HVAC system can be controlled to follow the regulation signals. Some researchers proposed using supply air fans with VFDs to provide fast regulation services [2][3][4] while others advocated controlling heat pumps with VFDs [5][6][7]. Different control methods were studied in [8] and it was shown that both fan speed and chilled water mass flow rate were effective control variables to provide frequency regulation services.

A two-step frequency regulation and energy imbalance scheduling algorithm is proposed in this paper. The symmetric and asymmetric frequency regulation service provision are carefully studied side-by-side. The simulation results show that our proposed frequency regulation provisioning scheme yields high performance score with minimal impact on the comfort level of the building occupants. This paper quantifies the impact of control parameters on the performance of both frequency regulation and climate control. The economic benefits of using building supply air fans to provide frequency regulation services are also carefully studied.

The rest of the paper is organized as follows. The framework of building EMS operations is described in Section II which includes energy baseline scheduling, frequency regulation service scheduling, and frequency regulation signal tracking. Detailed models for the building and HVAC systems are presented in Section III. The technical methodologies for day-ahead energy and frequency regulation scheduling and regulation signal tracking control are provided in Section IV. Simulation results are shown in Section V. The conclusions and future work are discussed in Section VI.

II. BUILDING EMS OPERATIONS FRAMEWORK

The building EMS operations framework is summarized below. In the day-ahead market time frame, the EMS of each commercial building determines the optimal hourly electricity consumption baseline and regulation capacity commitment for the next day. The objective of energy and frequency regulation scheduling is to maximize economic benefits of the commercial building based on the weather forecasts, the electricity price forecasts, the occupants' comfort preferences, and the HVAC system control model. The building EMS will send the energy and frequency regulation schedules to the distribution system operator (DSO) who performs aggregation and in turn sends the aggregated information to the transmission system operator (TSO).

In the hour-ahead or real-time market time frame, the electricity consumption baseline and regulation capacity commitment are continuously updated through a receding horizon control. The updated electricity consumption baseline and regulation capacity commitment are submitted to the market operators as self-schedules. To simplify the case study in this paper, it is assumed that the day-ahead scheduling results are the same as the hour-ahead/real-time scheduling results. By making this simplification, the real-time operations can be simulated based on the day-ahead schedules.

During the real-time operations, the TSO sends the frequency regulation signal for the aggregated building clusters to the DSO every 2 to 4 seconds. The DSO will disaggregate the signal and send it to the individual buildings. The AGC signal disaggregation process can follow that of generation allocation by using base points and participation factor [9]. The building EMS will control the HVAC system to track the frequency regulation signals.

III. COMMERCIAL BUILDING MODELING

A. Building Thermal Dynamics Model

A commercial building can be modeled as a group of connected zones, where each individual conditioned space is controlled by one thermostat. The building thermal dynamics can be captured by a resistor-capacitor (RC) circuit model. It is shown that a second-order RC model with two parameters is capable of reproducing the input-output behavior of a 13-state building (a single zone with 30 parameters) with high accuracy [10]. Thus, we simplify our previous model [11] by adopting the second-order RC model as follows:

$$C_w \dot{T}_w = \frac{T_a - T_w}{R_{wa}} + \frac{T_r - T_w}{R_{wr}} + \gamma G_s \qquad (1)$$

$$C_r \dot{T}_r = \frac{T_w - T_r}{R_{wr}} + Q_I + Q_{AC} \qquad (2)$$

where T_w, T_a, and T_r are the wall temperature, ambient temperature, and room temperature respectively. C_w and C_r are the thermal capacitance of the wall and the room air respectively. R_{wa} denotes the thermal resistance between the wall and the outside air. R_{wr} represents the thermal resistance between the wall and the room air. G_s denotes the solar irradiance. γ denotes the solar irradiance absorption factor.

Q_I denotes the internal heat gain. Q_{AC} represents the heat gain from the operations of the HVAC system.

B. HVAC System Model

The workflow of a typical single-zone HVAC system can be described as follows. In the air handling unit (AHU), outside air and part of the return air are mixed and then passed through a cooling or heating coil. Then the air is supplied to the zone by a supply air fan. The discharge air temperature is maintained at a preset point by varying the flow rate of chilled water or hot water passing through the coil. An indoor thermostat varies the discharge airflow rate to maintain the zone temperature at a preset work point. A building's heat gain provided by the HVAC system can be modeled as:

$$Q_{AC} = \dot{m}_a C_a (T_s - T_r) \qquad (3)$$

where $\dot{m}_a$, T_s, and C_a are the mass flow rate, temperature, and specific heat of the supply air respectively.

Most of the power in a HVAC system is consumed by the heater, the chiller, and the fan. Here we assume that heating power is provided by natural gas. Thus the total electricity power consumption of HVAC systems P_{AC} can be approximated by the sum of fan power P_f and chiller power P_c. The fan power is proportional to the cubic of its speed, i.e., $P_f(\dot{m}_a) = c_f \dot{m}_a^3$, where c_f is the fan power constant. The chiller's cooling load can be expressed as a function of the mass air flow rate and ambient temperature as $P_c(\dot{m}_a, T_a) = \dot{m}_a C_a (T_a - T_s)/COP$, where COP is the coefficient of performance for the chiller [11].

IV. TECHNICAL METHODOLOGIES

This section first derives the discrete-time building thermal dynamics model. The two-step energy baseline and frequency regulation capacity scheduling algorithm is also presented. At last the control method for regulation signal tracking is discussed in detail.

A. Model Discretization

Based on (1), (2), and (3), we can derive the continuous-time state-space model for the building's thermal dynamics.

$$\dot{\boldsymbol{x}}(t) = A^c \boldsymbol{x}(t) + B_1^c u(t) + B_2^c \boldsymbol{x}(t) u(t) + E^c \boldsymbol{d}(t) \qquad (4)$$

where $\boldsymbol{x}(t) = [T_w, T_r]^T$, $u(t) = \dot{m}_a$, and $\boldsymbol{d}(t) = [T_a, G_s, Q_I]^T$ are the state variables, input variable, and environmental variables respectively. A^c, B_1^c, B_2^c, and E^c are the coefficient matrices. Note that the bilinear term $\boldsymbol{x}(t)u(t)$ in (4) makes the model nonlinear and difficult to be discretized. However, when the state $\boldsymbol{x}(t)$ is known, the bilinear term can be linearized as follows:

$$\dot{\boldsymbol{x}}(t) = A^c \boldsymbol{x}(t) + B^c(t) u(t) + E^c \boldsymbol{d}(t) \qquad (5)$$

where $B^c(t) = B_1^c + B_2^c x(t)$ varies with the state $\boldsymbol{x}(t)$ over time. After zero-order-hold (ZOH) discretization, we can get the discrete-time time-variant model.

$$\boldsymbol{x}(k+1) = A\boldsymbol{x}(k) + B_k u(k) + E\boldsymbol{d}(k) \qquad (6)$$

where B_k varies with $\boldsymbol{x}(k)$.

The day-ahead scheduling problem formulation is inspired by the work in [12]. However, due to the nonlinearity of (6), it is difficult and time-consuming to solve the non-convex co-optimization problem in the day-ahead scheduling process. The size of the nonconvex optimization problem increases significantly when a building cluster is considered or when a complex RC model is used to represent a large-scale commercial building. To improve the computational efficiency, the day-ahead scheduling problem is formulated as a two-step optimization problem here. In the first step, an optimization problem is solved to determine the hourly power baselines. In the second step, the optimal hourly frequency regulation capacity commitment is determined. The simulation results show that the computation time can be reduced from 30 minutes to less than 4 minutes by switching from the co-optimization to a two-step sequential optimization process without significant loss of performance.

B. Power Baseline Scheduling

For the sake of simplicity, it is assumed that the HVAC system is working in a cooling mode only. The hourly power baseline can be determined by minimizing the electricity consumption cost, which can be formulated as follows:

$$\min_{u(k)} \sum_{k=1}^{96} LMP(k) \cdot P_{AC}(k) - \delta(k) \cdot \lambda(k) \cdot Reg_{max}(k) \quad (7)$$

subject to:

$$\boldsymbol{x}(k+1) = A\boldsymbol{x}(k) + B_k u(k) + E\boldsymbol{d}(k), \forall k \quad (8)$$

$$u_{min} \leq u(k) \leq u_{max}, \forall k$$

$$T_{min1}(k) \leq T_r(k) \leq T_{max1}(k), \forall k$$

$$P_{AC}(k) = P_f(u(k)) + P_c(u(k), T_a(k)), \forall k$$

$$\delta(k) = \max\{\lambda(k) - LMP(k), 0\}, \forall k$$

$$Reg_{max}(k) = \min\{P_f(u_{max}) - P_f(u(k)), P_f(u(k)) - P_f(u_{min})\}, \forall k$$

where k denotes the 15-minute time interval index. $LMP(k)$ and $\lambda(k)$ denote the forecasted locational marginal price for energy and regulation service at time interval k respectively. The term $LMP(k) \cdot P_{AC}(k)$ represents the electricity cost of the HVAC system at time interval k, and the term $\lambda(k) \cdot Reg_{max}(k)$ represents the revenue received from providing frequency regulation capacity at time interval k. $[u_{min}, u_{max}]$ denotes the input (mass air flow rate) range and $[\boldsymbol{T}_{min1}, \boldsymbol{T}_{max1}]$ is the range of comfortable temperatures. $\boldsymbol{T}_r$ and $\boldsymbol{T}_a$ are sub row vectors from matrices $\boldsymbol{x}$ and $\boldsymbol{d}$ respectively. To get the hourly scheduling results, the input should be kept unchanged within each hour by adding the constraint $u(k) = u(k+j), \forall k \in \Phi, \forall j \in \Psi$, where $\Phi = \{4m+1|0 \leq m \leq 23\}$ and $\Psi = \{1, 2, 3, 4\}$.

Note that $Reg_{max}(k)$ is the maximum potential for regulation capacity. It will be shown in Section V-D that the symmetrical regulation has minimal impact on the indoor temperature. Hence it is acceptable to relax the temperature constraints when estimating $Reg_{max}(k)$. The solution of an energy and frequency regulation scheduling co-optimization problem can be approximated by solving two optimization problems (7) and (9) in sequence. In solving the energy

baseline scheduling problem (7), the frequency regulation revenue is considered only when $\lambda(k)$ is higher than $LMP(k)$ by introducing the term $\delta(k)$. In other words, the frequency regulation service is provided only when it is more profitable than energy shifting service. In daily operations, $\delta(k)$ are rarely positive because during most of the hours $LMP(k)$ are higher than $\lambda(k)$.

C. Regulation Capacity Scheduling

After the hourly power baseline $\boldsymbol{u}^*$ is determined, the regulation capacity commitment can be determined by maximizing the frequency regulation revenue. The temperature bounds are loosened to $[\boldsymbol{T}_{min2}, \boldsymbol{T}_{max2}]$ where $T_{min2}(k) \leq T_{min1}(k)$ and $T_{max2}(k) \geq T_{max1}(k)$ for all k. It will be shown in the simulation results that most of the time the wider temperature bounds will not impact the occupants' comfort. This problem can be formulated as follows:

$$\max_{u_u(k), u_d(k)} \sum_{k=1}^{96} \lambda(k) \cdot Reg(k) \quad (9)$$

subject to :

$$\bar{\boldsymbol{x}}(k+1) = A\bar{\boldsymbol{x}}(k) + B_k(u^*(k) - \alpha u_d(k)) + E\boldsymbol{d}(k), \forall k \quad (10)$$

$$\underline{\boldsymbol{x}}(k+1) = A\underline{\boldsymbol{x}}(k) + B_k(u^*(k) + \alpha u_u(k)) + E\boldsymbol{d}(k), \forall k \quad (11)$$

$$u_{min} \leq u^*(k) - u_d(k), \ u^*(k) + u_u(k) \leq u_{max}, \forall k$$

$$u_u(k) \geq 0, \ u_d(k) \geq 0, \forall k$$

$$T_{min2}(k) \leq \underline{T}_r(k), \overline{T}_r(k) \leq T_{max2}(k), \forall k$$

$$Reg_{up}(k) = P_f(u^*(k)) - P_f(u^*(k) - u_d(k)), \forall k$$

$$Reg_{down}(k) = P_f(u^*(k) + u_u(k)) - P_f(u^*(k)), \forall k$$

$$Reg(k) = Reg_{up}(k) = Reg_{down}(k), \forall k \quad (12)$$

where $\bar{\boldsymbol{x}}$ and $\underline{\boldsymbol{x}}$ are the upper and lower temperature bounds. $\overline{\boldsymbol{T}}_r$ and $\underline{\boldsymbol{T}}_r$ are sub row vectors from matrices $\bar{\boldsymbol{x}}$ and $\underline{\boldsymbol{x}}$. Here we consider the regulation operation under the Pennsylvania-New Jersey-Maryland Interconnection (PJM) market, and the dynamic regulation signal (RegD[13]) is used as the reference signal. As discussed in [14], the regulation signal's 15-minute average are much smaller than 1. After analyzing one year of historical RegD signal from PJM market, we found that the average change requested by RegD over 15 minutes is less than 10% of the regulation capacity with 95% probability. Therefore, we set $\alpha = 0.1$ in our simulation. Thus $\bar{\boldsymbol{x}}$ and $\underline{\boldsymbol{x}}$ can be estimated by (10) and (11). At time interval k, $u_d(k)$ and $u_u(k)$ represent the input decrement and increment. $Reg_{up}(k)$ and $Reg_{down}(k)$ denote the regulation up (power decrement) capacity and regulation down (power increment) capacity. Constraint (12) is used to make the regulation capacities symmetric. To get the hourly scheduling results, the regulation capacity should be kept unchanged within each hour by adding the constraint $u_u(k) = u_u(k+j), u_d(k) = u_d(k+j), \forall k \in \Phi, \forall j \in \Psi$.

D. Nonlinear Optimization Problem

Note that (8), (10), and (11) are time-variant state-space equations due to B_k. A sequential programming approach is adopted to solve the nonlinear scheduling problems (7) and (9). For example, the sequential optimization approach

for solving (7) is depicted in Fig. 1. As shown in the flowchart, in the first step, the state vector is initialized as $\boldsymbol{x_0} = [\boldsymbol{T}_{w0}^T, \boldsymbol{T}_{r0}^T]^T$, where $\boldsymbol{T}_{w0} = \boldsymbol{T}_{r0} = 0.5(\boldsymbol{T}_{min1} + \boldsymbol{T}_{max1})$. In this initialization, both the wall temperature and the room temperature are assumed to be in the center of comfortable temperature range for all time intervals. In the next step, B_k is derived based on $\boldsymbol{x_0}(k)$ for all k. Afterwards, $u^*(k)$ is calculated by solving the optimization problem (7). For better convergence, the window of variation for decision variable $u(k)$ and state variable $T_r(k)$ between two iterations are limited by $\Delta u(k)$ and $\Delta T_r(k)$, where $\Delta u(k)$ is exponentially decreasing over time and $\Delta T_r(k)$ is a constant. At last, the state vector $\boldsymbol{x}(k)$ is updated by $u^*(k)$. The process is repeated with updated $\boldsymbol{x}(k)$ until the convergence condition is met. $\boldsymbol{u}^*$ is the desired output. A similar approach can be taken to solve the nonlinear scheduling problem (9).

Note that to speed up the algorithm, it is preferable to transform the nonlinear optimization problem into sequential quadratic programming (SQP) [15] or sequential linear programming (SLP) [16] problems by first-order or second-order Taylor expansion. It should be emphasized that global optimal solution(s) cannot be guaranteed due to the non-convexity of the original problem.
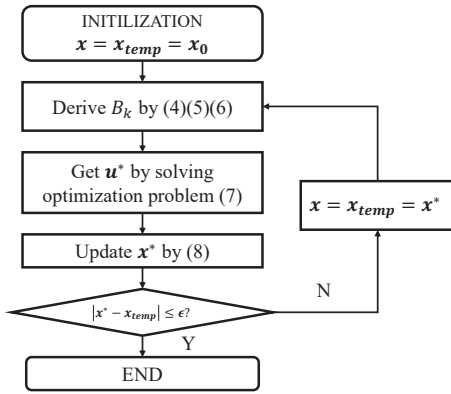

Fig. 1. Flowchart for power baseline scheduling algorithm

E. Regulation Signal Tracking Control

The control architecture is adapted from [2], where the supply air fan's power is regulated to track the regulation signal. As shown in Fig. 2, a feedforward controller (regulation controller) is integrated to change the VFD command to the supply air fan so that the deviation in power consumption tracks the regulation reference, and a proportional-integral (PI) feedback controller in the thermostat is used to reduce the bias from desired room temperature. Since the chiller's time constant is typically greater than 200 seconds, its effect on power consumption and indoor climate is neglected here. The dynamics of the fan and the duct system are simplified as first-order plants, which are described in details in [2].

V. CASE STUDY

A. Simulation Setup

Most of the parameters for the building and HVAC system can be found in [11], and parts of them are adjusted to repre-
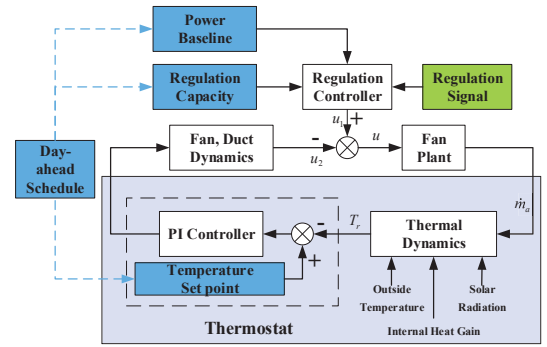

Fig. 2. Schematics of the regulation signal tracking control

sent a typical medium office building. The simulated building model's dimension is adjusted to $70m \times 70m \times 10.8m$, and the fan's air flow rate ranges from $1kg/s$ to $31kg/s$, with a maximum power of $50kW$. The weather information is taken from EnergyPlus weather data on 9/15/1999 at Riverside, California. The forecasted energy prices and regulation capacity prices are taken from PJM market's historical data. $[\boldsymbol{T}_{min1}, \boldsymbol{T}_{max1}]$ are set to $[20, 23]\,°C$ during working hours (7:00 A.M. - 10:00 P.M.) and $[15, 30]\,°C$ during non-working hours. $[\boldsymbol{T}_{min2}, \boldsymbol{T}_{max2}]$ are set to $[19, 25]\,°C$ during working hours and $[10, 40]\,°C$ during non-working hours.

To evaluate the regulation performance, the continuous bilinear building model (4) and proposed control strategies are implemented in MATLAB/Simulink. The default PI controller's parameters are set to $P = 0.5$ and $I = 10^{-5}$. To evaluate the regulation performance, the performance scores defined in PJM market are calculated hourly, which consist of three parts, namely the correlation score S_c, the delay score S_d, and the precision score S_p [13]. The total performance score S_t is the average of these three scores. With the regulation capacities as weights, the weighted averages of hourly performance scores are adopted here to reflect the regulation performance for a whole day.

B. Day-ahead Scheduling and Real-time Operations

The day-ahead scheduling results are shown in Fig. 3, which indicates that the maximum regulation capacity can reach around 40% of the fan's maximum power. The expected temperature curves are shown in Fig. 4, where T_{lb} and T_{ub} denote the expected lower and upper temperature bounds during regulation respectively, and T_{base} denotes the expected temperature curve without regulation. It is evident that all three curves are within the desired temperature boundaries.

As shown in Fig. 4, the fan's power deviation can follow the regulation signal very well during real-time operations. The weighted average of each performance scores are $S_c = 0.999$, $S_d = 0.967$, $S_p = 0.913$, and $S_t = 0.959$. The high performance scores demonstrated the effectiveness of the proposed control scheme.

C. Co-Scheduling Versus Two-step Scheduling

It is also possible to schedule both power baseline and regulation capacity in a co-scheduling process by combining

the optimization problems stated in Sections IV-B and IV-C. However, due to the complexity of the co-scheduling model, the combination easily leads to oscillation effects. For example, the co-scheduling problem still oscillates after 200 iterations (around 30 minutes) with SLP algorithm. On the other hand, the proposed two-step scheduling problem converges quickly. The power baseline scheduling problem converges in 235.56 seconds with 17 iterations, and the frequency reserve scheduling problem converges in 35.36 seconds with three iterations. The results of co-scheduling after 50 iterations are $80.24 (energy cost) and $3.38 (regulation revenue), while the results of two-step scheduling are $80.80 (energy cost) and $3.64 (regulation revenue), which is very close to the results of the co-scheduling problem. Therefore, it is better to adopt the proposed two-step scheduling algorithm in real-time smart building operations because local optimal solution(s) can be obtained in much shorter time. All the above problems are solved on a Windows PC with 2.1 GHz CPU and 8 GB memory.
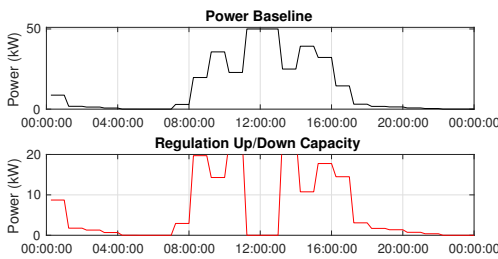

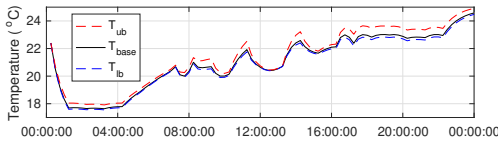Fig. 3. Frequency Regulation up/down capacity and power baseline

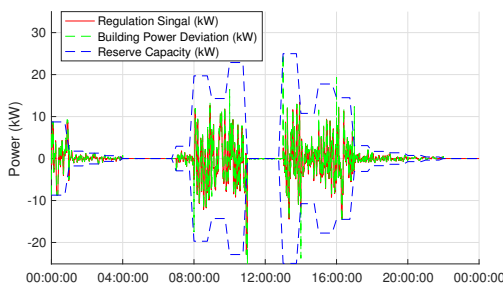Fig. 4. Expected temperature curves

Fig. 5. Frequency regulation performance for a whole day

D. Impact of Frequency Regulation on Indoor Climate

To study the impact of frequency regulation on indoor climate, two simulations are performed. The first simulation case is with frequency regulation provisions and the second case is without frequency regulation provisions (the regulation signal is set to zero). As shown in Fig. 6 the temperature deviation between the two cases is very close to zero and the absolute deviation is less than $0.73°C$. The small deviation in temperature is mainly due to the mean reverting and symmetric frequency regulation (RegD) signals in PJM market. Note that many independent system market
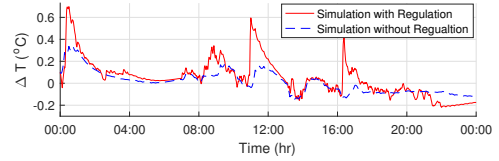

Fig. 6. Temperature deviation trajectory with symmetric regulation

operator such as California Independent System Operator (CAISO) have separate markets for frequency regulation up and down services. If the symmetric frequency regulation capacity constraints (12) is removed, then the scheduled regulation down capacity would be much larger than frequency regulation up capacity. In this scenario, the maximum temperature deviation can be as high as $6.1°C$ as shown in Fig. 7. Moreover, the frequency regulation signal is not mean-reverting in the CAISO market, which could further enlarge the temperature deviation. Thus the coefficient α in (10) and (11) should be set close to 1.

Note that the building frequency regulation scheduling strategy should be different for different electricity markets. In a single frequency regulation product market like the PJM, the building can provide symmetric regulation services with little impact on its indoor climate. In a frequency regulation market with two products like the CAISO, the building should operate close to the temperature upper limit and mainly provide frequency regulation down service. These rules can help us determining the two temperature bounds for the two-step optimization problem to get a closer solution to the global optimal solution.
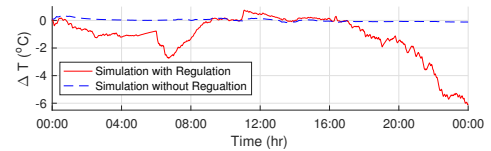

Fig. 7. Temperature deviation trajectory with asymmetric regulation

E. Frequency Regulation and Climate Control Performances

As shown in Fig. 2, the input signal u for the fan plant is composed of the feedforward control component u_1 and the feedback control component u_2. Thus the frequency regulation performance and climate control performance are coupled. This section studies the impact of PI controllers' parameters on the frequency regulation and climate control performances when we fix the settings for the regulation controller. To perform this study, simulations are conducted with different pairs of proportionality coefficient P and integral

coefficient I, which are selected for easier comparison and analysis. Four frequency regulation performance indices (S_c, S_d, S_p, and S_t) and one climate control performance index (S_{con}) are calculated to quantify the frequency regulation and climate control performances. S_{con} is the climate control performance score which is calculated as $1 - Err_{con}$, where Err_{con} is the mean absolute percentage error of temperature deviation from temperature set points.

As shown in Table I, if only the feedforward control component (u_1 in Fig. 2) is implemented ($P = 0$, $I = 0$, no feedback control), the frequency regulation performance is the best, while the climate control performance is the worst due to the model error. If the feedback control component (u_2 in Fig. 2) is strengthened by increasing P, the climate control performance improves, while the frequency regulation performance degrades.

Note that the climate control performance is worse when I increases from 0 to 10^{-5}. This is because the delay introduced by system's fan and duct systems is significant, which increases the integral errors. A Smith predictor [3] can help mitigate this problem. In summary, there exists a trade-off between the frequency regulation performance and climate control performance which should be carefully considered during the control parameter tuning process.

TABLE I
FREQUENCY REGULATION VERSUS CLIMATE CONTROL PERFORMANCE

Coefficients		Performance Indices				
P	I	S_c	S_d	S_p	S_t	S_{con}
0	0	0.999	0.967	0.957	0.974	0.311
0.1	0	0.999	0.967	0.956	0.974	0.330
0.5	0	0.999	0.967	0.938	0.968	0.395
1	0	0.998	0.967	0.909	0.958	0.456
0	10^{-5}	0.999	0.967	0.927	0.964	0.289
0.1	10^{-5}	0.999	0.967	0.926	0.964	0.313
0.5	10^{-5}	0.999	0.967	0.913	0.959	0.387
1	10^{-5}	0.998	0.967	0.893	0.952	0.451

F. Economic Benefits

A 24-hour simulation is conducted for the test building. The total electricity cost for the fan and chiller is about \$80.8 and the revenue received from providing symmetric frequency regulation service is about \$3.64. The average frequency regulation capacity provision is about 6.15 kW.

VI. CONCLUSIONS AND FUTURE WORK

This paper proposes a two-step frequency regulation and energy scheduling algorithm and a regulation signal tracking control mechanism to provide frequency regulation via commercial buildings. The proposed scheduling and control algorithm is not only computationally efficient but also yields high frequency regulation performance scores. The analytical results suggest that buildings should select different frequency regulation scheduling strategy in the electricity markets based on the answer to two questions. First, is there an equal capacity constraint on frequency regulation up and down? Second, is the frequency regulation signal mean reverting? The day-ahead and real-time operation simulations

of the building HVAC system also suggest that control parameters should be carefully selected to strike a balance between frequency regulation control performance and climate control performance. At last, the economic benefits of providing frequency regulation for a typical medium office building is quantified in the PJM market.

The impact of load forecast errors and environmental disturbances on frequency regulation performance will be considered in our future work. In addition, realistic power distribution system operating constraints and losses [17] will be considered in the building aggregation process.

REFERENCES

[1] B. Kirby, "Ancillary services: Technical and commercial insights," 2007. [Online]. Available: http://www.science.smith.edu/%7Ejcardell/Courses/EGR325/Readings/Ancillary%5FServices%5FKirby.pdf

[2] H. Hao, Y. Lin, A. S. Kowli, P. Barooah, and S. Meyn, "Ancillary service to the grid through control of fans in commercial building HVAC systems," *IEEE Trans. Smart Grid*, vol. 5, no. 4, pp. 2066–2074, Jul. 2014.

[3] Y. Lin, P. Barooah, and S. P. Meyn, "Low-frequency power-grid ancillary services from commercial building HVAC systems," in *2013 IEEE Int. Conf. Smart Grid Communications*, Oct. 2013, pp. 169–174.

[4] M. Maasoumy, J. Ortiz, D. Culler, and A. Sangiovanni-Vincentelli, "Flexibility of commercial building hvac fan as ancillary service for smart grid," *ArXiv e-prints*, Nov. 2013. [Online]. Available: http://arxiv.org/abs/1311.6094

[5] Y. J. Kim, L. K. Norford, and J. L. Kirtley, "Modeling and Analysis of a Variable Speed Heat Pump for Frequency Regulation Through Direct Load Control," *IEEE Trans. Power Syst.*, vol. 30, no. 1, pp. 397–408, Jan. 2015.

[6] L. Su and L. K. Norford, "Demonstration of HVAC chiller control for power grid frequency regulation - Part 1: Controller development and experimental results," *Science and Technology for the Built Environment*, vol. 21, no. 8, pp. 1134–1142, Nov. 2015. [Online]. Available: http://www.tandfonline.com/doi/full/10.1080/23744731.2015.1072449

[7] E. Vrettos and G. Andersson, "Scheduling and provision of secondary frequency reserves by aggregations of commercial buildings," *IEEE Trans. Sustain. Energy*, vol. 7, no. 2, pp. 850–864, Apr. 2016.

[8] P. Zhao, G. P. Henze, M. J. Brandemuehl, V. J. Cushing, and S. Plamp, "Dynamic frequency regulation resources of commercial buildings through combined building system resources using a supervisory control methodology," *Energy and Buildings*, vol. 86, pp. 137–150, Jan. 2015.

[9] A. J. Wood, B. F. Wollenberg, and G. B. Sheble, *Power Generation, Operation, and Control*. John Wiley & Sons, 2014.

[10] Y. Lin, T. Middelkoop, and P. Barooah, "Issues in identification of control-oriented thermal models of zones in multi-zone buildings," in *51st IEEE Conf. Decision and Control*, Dec. 2012, pp. 6932–6937.

[11] J. Shi, N. Yu, and W. Yao, "Energy efficient building HVAC control algorithm with real-time occupancy prediction," in *Int. Conf. Sustainability in Energy and Buildings*, Sep. 2016.

[12] E. Vrettos, E. C. Kara, J. MacDonald, G. Andersson, and D. S. Callaway, "Experimental demonstration of frequency regulation by commercial buildings - Part II," *ArXiv e-prints*, May 2016. [Online]. Available: http://arxiv.org/abs/1605.05558

[13] PJM, *PJM manual 12: Balancing operations*, Dec. 2015. [Online]. Available: http://www.pjm.com/%7E/media/documents/manuals/m12.ashx

[14] E. Vrettos, E. C. Kara, J. MacDonald, G. Andersson, and D. S. Callaway, "Experimental demonstration of frequency regulation by commercial buildings - Part I," *ArXiv e-prints*, May 2016. [Online]. Available: http://arxiv.org/abs/1605.05835

[15] P. T. Boggs and J. W. Tolle, "Sequential quadratic programming," *Acta numerica*, vol. 4, pp. 1–51, 1995.

[16] R. E. Griffith and R. A. Stewart, "A nonlinear programming technique for the optimization of continuous processing systems," *Management Science*, vol. 7, no. 4, pp. 379–392, 1961.

[17] W. Wang and N. Yu, "LMP decomposition with three-phase DCOPF for distribution system," in *2016 IEEE Innovative Smart Grid Technologies - Asia*, Nov. 2016, pp. 1-8.